RSC Advances

PAPER

View Article Online
View Journal | View Issue

Cite this: *RSC Adv.*, 2018, **8**, 18451

Facile synthesis of an urchin-like Sb_2S_3 nanostructure with high photocatalytic activity†

Jing Zhou, *[ab] Jiangchun Chen,[ab] Mengyao Tang,[ab] Yanqun Liu,[ab] Xiaoyu Liu[ab] and Hua Wang *[ab]

Received 19th December 2017
Accepted 23rd April 2018

DOI: 10.1039/c7ra13392h

rsc.li/rsc-advances

Herein, an urchin-like Sb_2S_3 nanostructure has been synthesized without a surfactant *via* a wet chemical method. The crystal structure, morphology, composition and optical properties were characterized using XRD, TEM, SEM, EDS, Raman spectroscopy, and diffuse reflectance absorption spectroscopy. The factors, including the reaction time, temperature, and ratio of the raw materials, influencing the evolution of the urchin-like morphology have been discussed, and a plausible formation mechanism for the urchin-like Sb_2S_3 has been proposed. The urchin-like Sb_2S_3 micro/nanostructure exhibits high catalytic performance towards the degradation of MB under visible light irradiation. The photodegradation ratio of MB is up to 99.32% under visible light irradiation of 130 min. Our synthesis method will be extended to prepare other photocatalysts.

In recent years, nanomaterials with controllable size and novel morphologies have been extensively studied due to their unique physical and chemical properties.[1–5] For instance, AgBr nanoplates,[6] AgCl octahedrons[7] and $NaTi_2(PO_4)_3$ nanocubes[8] show unique photocatalytic activities and electrochemical performances. Hierarchical flower-like SnO_2 nanospheres[9] or TiO_2 nanorod arrays[10,43] exhibit highly efficient gas sensing and photoelectrochemical properties.

As an important V–VI compound, antimony sulfide (Sb_2S_3) is considered as a promising material for energy conversion due to its suitable band gap (1.5–2.2 eV), which covers the range of the solar spectrum.[11–13] To the best of our knowledge, Sb_2S_3 nanomaterials with different morphologies have been mainly synthesized using various surfactants.[14] Surfactants can regulate the morphology and structure of the nanoparticles effectively by parceling on the surface of the particles through the coordination or charge effect.[15] By adding surfactants such as cetyltrimethylammonium bromide (CTAB),[16] polyethylene glycol (PEG),[17] dodecyltrimethylammonium bromide (DTAB)[18] and polyvinylpyrrolidone (PVP),[19–21] some nanostructures including straw-tied-like, nanorod[22,23], nanosheet,[24] nanotube, dandelion-like, double cauliflower-like,[25] bar,[26] dumbbell-like, and nanowire bundle structures have been successfully prepared, which show potential applications in photocatalysis and energy storage areas. However, how to effectively synthesize Sb_2S_3 crystals and control their morphology *via* a simple method is still challenging for materials scientists. Herein, we report a simple wet chemical method to synthesize an urchin-like Sb_2S_3 nanostructure without any surfactant. Moreover, we have examined the photocatalytic activity of Sb_2S_3 by the degradation of MB under simulated visible light irradiation. Our study presents an Sb_2S_3 nanostructure with good application in the visible-light photocatalytic field.

The morphology and size of the products were revealed by the SEM and TEM images. Fig. 1a shows the SEM image of the urchins-like Sb_2S_3 prepared under refluxing conditions at 160 °C for 5 h. The as-prepared Sb_2S_3 products mainly consist of the uniform urchin-like structure. The magnified SEM image shows that the urchin-like structure consists of nanorods stretching radially from the same central point (Fig. 1b). The TEM image further confirms that the urchin-like Sb_2S_3 is made up of many individual nanorods with lengths about 10 μm and diameters of 100 nm (Fig. 1b and c). The measured spacing of the crystallographic planes is 0.309 nm, which is consistent with the (320) plane lattice distance of orthorhombic Sb_2S_3 (Fig. 1d).

The XRD pattern of the obtained sample is shown in Fig. 1e. All the diffraction peaks in the XRD pattern can be readily indexed to orthorhombic Sb_2S_3 (JCPDS no. 42-1393) with the calculated lattice parameters of $a = 1.120$ nm, $b = 1.128$ nm and $c = 0.383$ nm. No characteristic peaks for impurities are observed. The fact that the reflection peaks of Sb_2S_3 are strong and sharp indicates that Sb_2S_3 is highly crystalline (Fig. 1e). The EDS spectrum reveals that the as-prepared products consist of S and Sb elements, and the observed C and Cu peaks are due to the carbon-coated Cu grid[27] (Fig. 1f). Furthermore, the elemental distribution ratio of S and Sb in the compound was

[a]*College of Chemistry Engineering, Northeast Electric Power University, Jilin 132012, P. R. China. E-mail: zhoujing@mail.nedu.edu.cn*

[b]*School of Chemistry, Beihang University, Beijing 100191, P. R. China. E-mail: wanghua8651@buaa.edu.cn*

† Electronic supplementary information (ESI) available: Synthetic process and mechanism analysis. See DOI: 10.1039/c7ra13392h

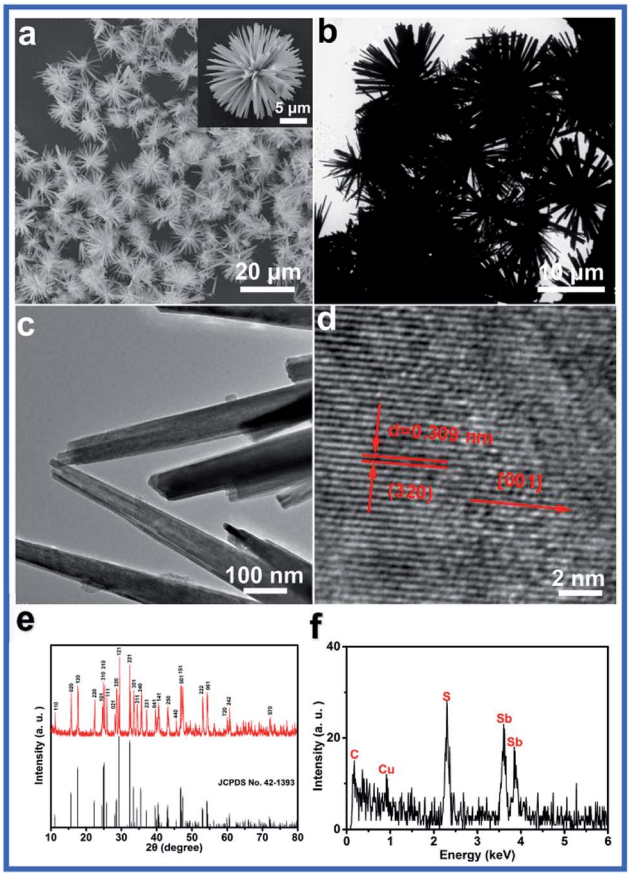

Fig. 1 (a) SEM, (b and c) TEM and (d) HRTEM images, (e) XRD pattern and (f) EDS spectrum of urchin-like Sb_2S_3.

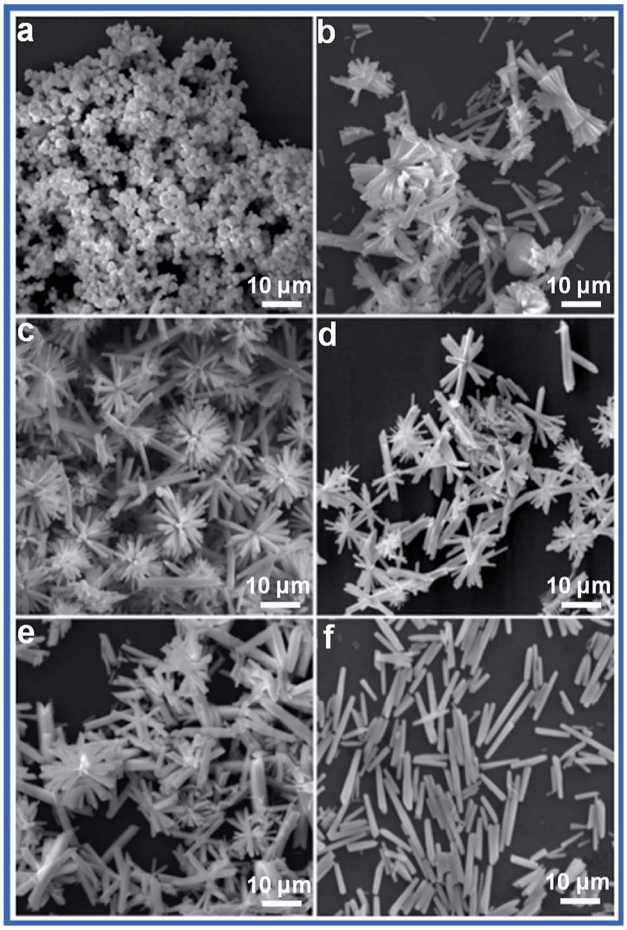

Fig. 2 SEM images of the Sb_2S_3 prepared at 160 °C for different times: (a) 2 h, (b) 3 h, (c) 6 h, (d) 9 h, (e) 12 h, and (f) 15 h.

found to be about 3 : 2 through the quantification calculation of the EDS peaks, which was consistent with the chemical formula of antimony sulfide.[28]

The effects of the reaction time, reaction temperature and the ratio of the raw materials on the as-obtained products were carefully studied to investigate the formation of the urchin-like morphology. Fig. 2 reveals the SEM images of the as-obtained samples prepared at different reaction times. Initially, no product was formed. When the reaction time was prolonged to 2 h, amorphous antimony sulfide was formed (Fig. 2a). After 3 h, single units with slight splitting were observed (Fig. 2b). Upon increasing the reaction time, uniform urchin-like Sb_2S_3 was obtained. When the reaction time was further increased to 6 h, the urchin-like structure was transformed into a rod-flower structure in which the thorns of the urchin-like structure were thicker (Fig. 2c). As shown in Fig. 2d and e, after 9 h, the rod-flower structure began to rupture and finally converted into irregular nanorods with lengths of about 15 μm, as shown in Fig. 2f.

The reaction temperature also has a significant effect on the morphologies of the final products. As shown in Fig. 3a, amorphous nanoparticles with an irregular shape were formed at 140 °C. When the temperature was increased to 150 °C, a simple splitting phenomenon appeared. Upon further increasing the temperature, the urchin-like micro/nanostructure was formed. A further increase in the reaction temperature led to the formation of rod flowers. When the reaction temperature was 180 °C, some rod-like structures appeared.

We examined the effect of the ratio of the raw materials on the product. Only rod particles were observed at a ratio of S/Sb = 1 : 1 (Fig. 4a). When the ratio was increased to 1 : 3, the urchin shapes were observed. A further increase in the concentration of the sulfur source led to the appearance of nest structures. Irregular spherical particles were finally generated when the ratio of the raw materials was 1 : 7.

Based on the experimental results, a plausible reaction for the synthesis of the Sb_2S_3 crystals can be interpreted as follows:

$$CH_3CSNH_2 + 2OH^- \rightarrow S^{2-} + CH_3COO^- + NH^{4+} \quad (1)$$

$$[Sb_2(C_4H_4O_6)_2]^{2-} \rightarrow 2Sb^{3+} + 2(C_4H_4O_6)^{4-} \quad (2)$$

$$2Sb^{3+} + 3S^{2-} \rightarrow Sb_2S_3\downarrow \quad (3)$$

According to the abovementioned experimental results, we speculated the formation mechanism of the urchin-like Sb_2S_3 structure. Sb_2S_3 is a highly anisotropic semiconducting material

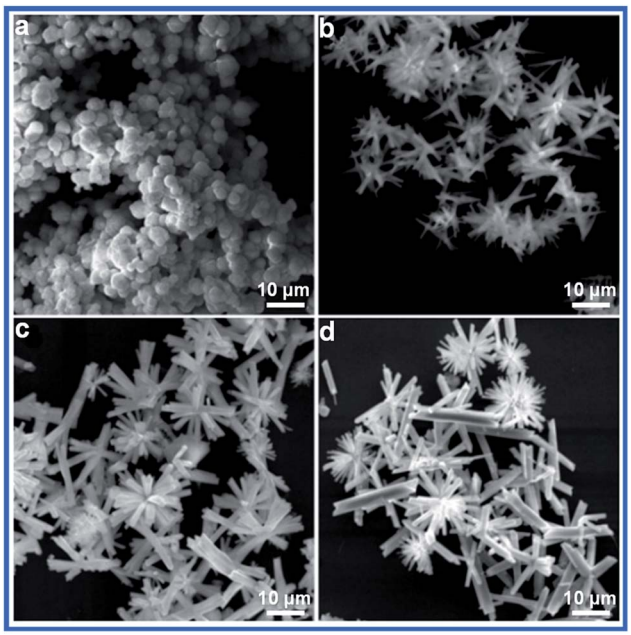

Fig. 3 SEM images of Sb_2S_3 prepared for 5 h at different reaction temperatures: (a) 140 °C, (b) 150 °C, (c) 170 °C and (d) 180 °C.

with infinite ribbon-like (Sb_4S_6) polymers and layers in its orthorhombic crystal structure.[29,30] As already reported in the literature, Sb_2S_3 tends to easily form one-dimensional nanorods along the *c*-axis due to intermolecular attraction between the antimony and sulfur atoms.[31–34] Because of the fast and anisotropic crystal growth, many newborn clusters agglomerate together to deposit on a particular particle face, causing crystal splitting when the solution is in the excess saturation state.[35,36] Then, each of the nanorods starts to grow into urchin-like crystals. This is similar to the chain-like crystalline structure of Bi_2S_3; this further ascertains that Sb_2S_3 has a strong splitting ability.[37,38] Our research suggests that the degree of splitting is increased when the reaction time is prolonged. In the subsequent stage, the nanorods are detached from the urchin-like structures; this results in well-dispersed nanorods due to the instability of the surface energy.[39] The whole process of this morphological evolution is shown schematically in Fig. 5. The amorphous nanoparticles of Sb_2S_3 appeared with no splitting. Upon increasing the reaction time, the Sb_2S_3 nanostructures change from small sheaves with simple splitting to urchin-like structures.

The fact that the optical properties of the as-prepared Sb_2S_3 are determined using the absorption spectrum (Fig. 6a) provides a simple and effective method to estimate the band gap of the urchin-like Sb_2S_3.[40,41] The band gap value of 1.64 eV determined by other researchers is quite comparable to the values reported in the bibliographical information.[42] Furthermore, it can be seen that optical absorption occurs in nearly all the visible light region; this suggests that the as-synthesized Sb_2S_3 can be stimulated by visible light. Raman spectrum of the urchin-like Sb_2S_3 is shown in Fig. 6b. The appearance of sharp peaks at 147, 198, 257, 305, and 452 cm^{-1} suggests the formation of a highly crystalline product, which is consistent with the XRD results.[43] Due to suitable band gap of urchin-like Sb_2S_3, the photocatalytic activity of urchin-like Sb_2S_3 was assessed by depositing an organic dye (MB) in an aqueous solution under visible light irradiation. The concentration of MB dye was monitored at 665 nm using an UV/vis spectrophotometer. From the blank experiment (Fig. S2†), we can see a slight drop in the curve due to self-degradation of MB dye under visible light irradiation. Therefore, we can conclude that the dye is almost photo-stable under these conditions. It can be clearly observed from Fig. 6c that the organic dye is slightly degraded by Sb_2S_3 in the dark. According to Fig. 6d, the organic dye could be degraded by only 23.1% using H_2O_2, whereas the degradation efficiency for MB dye was 99.34% in the presence of Sb_2S_3 and H_2O_2 after 130 min; this indicated that the degradation of the organic dye was mainly attributed to the excellent

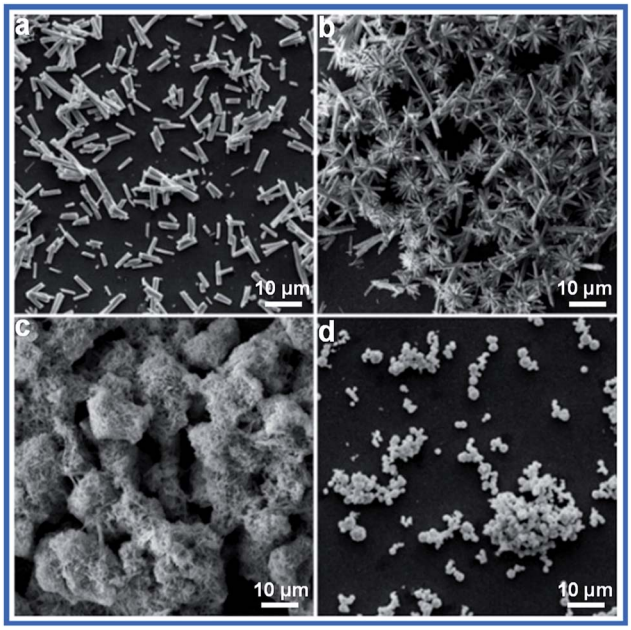

Fig. 4 SEM images of Sb_2S_3 prepared with different ratios of S and Sb: (a) S/Sb = 1 : 1, (b) S/Sb = 1 : 3, (c) S/Sb = 1 : 5, and (d) S/Sb = 1 : 7.

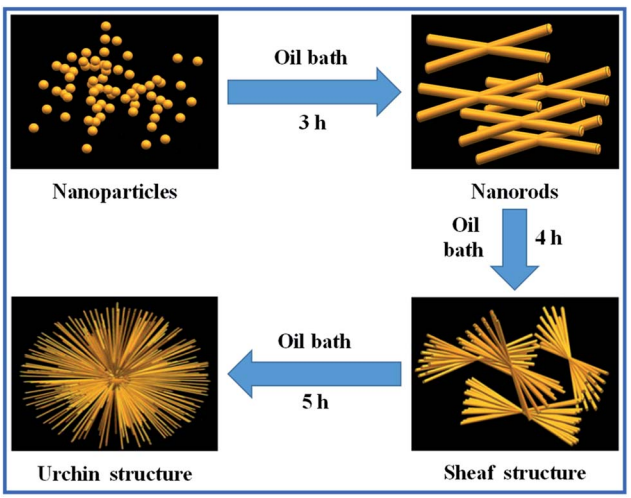

Fig. 5 A schematic of the formation of the urchin-like Sb_2S_3 structure.

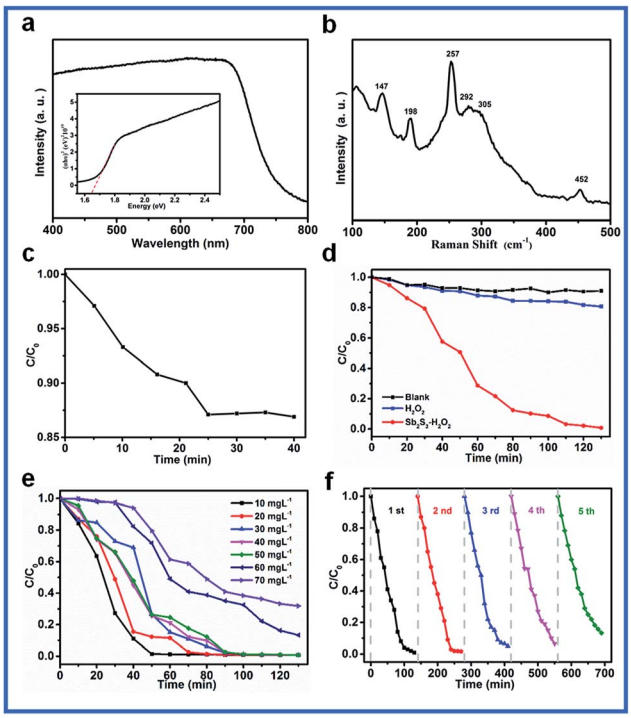

Fig. 6 (a) The diffuse reflectance absorption spectrum of the as-prepared Sb_2S_3 sample (the inset presents the corresponding plots of $(\alpha h\nu)^2$ *versus* photon energy). (b) The room-temperature Raman spectrum. (c) The degradation curve for MB in the dark. (d) The degradation curves for MB using the different catalyst systems (e) the degradation curves at different MB concentrations. (f) The cycling runs for the degradation of MB.

photocatalytic activity of Sb_2S_3. The photoluminescence spectra of the as-prepared urchin-like Sb_2S_3 shows a low signal, suggesting the good charge separation properties of our samples (Fig. S1a†). Fig. S1b† shows the *I–T* curves of the FTO/Sb_2S_3 photoelectrode, of which the photocurrent intensity is 36.057 μA cm^{-2} at a potential of 0 V *versus* Ag/AgCl, and this fast photocurrent response is consistent with the PL results. Fig. 6e shows the photocatalytic degradation of an aqueous solution of MB at different concentrations by urchin-like Sb_2S_3. However, with an increase in the concentration of MB, the degradation efficiency is reduced. Furthermore, the cycling performance of urchin-like Sb_2S_3 was measured using the same photodegradation process. The photocatalyst was obtained by centrifugation and washed with deionized water after each cycle. The degradation ratio decreased slightly after reuse for 5 times; the slight decay in the photodegradation activity was partially ascribed to the inevitable loss of the photocatalyst during the washing and centrifugation process; this suggested that Sb_2S_3 exhibited prominent photocatalytic stability (Fig. 6f).

The promising photocatalytic activity of Sb_2S_3 can be mainly attributed to its relatively narrow band gap (1.64 eV), making it a perfect photocatalyst to efficiently absorb and utilize visible-light energy. As is known, the urchin-like nanostructure has been extensively investigated due to its potential applications in many areas such as in varistors, electronic devices, UV-absorbers, and catalysis.[47,48] This kind of nanostructure has a high specific surface area, which endows it with a large contact area with the dye and superior light harvesting efficiency in the field of photocatalysis.[49] Moreover, the single crystalline nanorod-assembled urchin-like nanostructure is favorable for fast electron transfer and thus facilitates electron and hole separation.[46,50,51] In particular, when urchin-like Sb_2S_3 is irradiated by visible light of energy greater than its band gap, electron–hole pairs will be generated and partially separated. The electrons and holes react with the adsorbed surface substances, such as O_2 and OH^-, to form the reactive species $\cdot O^{2-}$, $\cdot OH$, which are the major oxidative species in the decomposition of organic pollutants. Then, the oxidative species degrade the organic pollutant into small molecules such as CO_2 and H_2O.[44,45] *p*-Benzoquinone (BQ) and isopropyl alcohol (IPA) were used as additive agents to trap the active species $\cdot O_2^-$ and $\cdot OH$, respectively. Fig. S2† shows the degradation curves for MB after the addition of the different capture agents. It can be seen that IPA has a significant inhibitory effect on the degradation of MB, whereas the effect of BQ is less; this indicates that $\cdot OH$ plays a major role in the photocatalytic process.

The degradation of the organic dye was accomplished *via* a series of parallel and consecutive redox reactions as show in eqn (2.1)–(2.5).

$$Sb_2S_3 + h\nu \rightarrow Sb_2S_3 (h_{VB}^+ + e_{CB}^-) \quad (2.1)$$

$$O_2 + e_{CB}^- \rightarrow \cdot O_2^- \quad (2.2)$$

$$H_2O \rightarrow H^+ + OH^- \quad (2.3)$$

$$OH^- + h_{VB}^+ \rightarrow \cdot OH \quad (2.4)$$

$$MB + \cdot OH + \cdot O^{2-} \rightarrow CO_2 + H_2O + \ldots \quad (2.5)$$

In summary, an urchin-like Sb_2S_3 nanostructure was successfully prepared without surfactants using a wet chemical method. The corresponding crystal splitting formation mechanism of urchin-like Sb_2S_3 was tentatively suggested. The narrow band gap of the urchin-like Sb_2S_3 was evaluated to be 1.64 eV, which was close to the best photoelectric conversion value reported to date. In addition, urchin-like Sb_2S_3 exhibited excellent photocatalytic performance; the degradation efficiency for the organic dye was 99.34% after exposure to visible-light irradiation for 130 min. The high photocatalytic activity of Sb_2S_3 was mostly due to its narrow band gap and wide absorption range of visible light. Our investigation demonstrates that Sb_2S_3 with urchin-like nanostructures has great potential to be applied in the degradation of organic contaminants.

Conflicts of interest

There are no conflicts to declare.

Acknowledgements

The authors acknowledge the financial support provided by the Natural Science Foundation of China (No. 51772049).

Notes and references

1 N. E. Kelly, S. O. Lee and K. D. Harris, *J. Am. Chem. Soc.*, 2001, **123**, 12682.
2 A. M. Morales and C. M. Lieber, *Science*, 1998, **279**, 208.
3 X. Peng, L. Manna and W. Yang, *Nature*, 2000, **404**, 59.
4 A. P. Alivisatos, *Science*, 1996, **271**, 933.
5 H. Dai, E. W. Wong and Y. Z. Lu, *Nature*, 1995, **375**, 769.
6 H. Wang, J. Gao, T. Q. Guo, R. M. Wang and L. Guo, *Chem. Commun.*, 2012, **48**, 275.
7 H. Wang, X. F. Lang, R. Hao, L. Guo, J. H. Li, L. H. Wang and X. D. Han, *Nano Energy*, 2016, **19**, 8.
8 J. Yang, H. Wang, P. F. Hu, J. J. Qi, L. Guo and L. H. Wang, *Small*, 2015, **31**, 3744.
9 H. Wang, Q. Q. Liang, W. J. Wang, Y. R. An, J. H. Li and L. Guo, *Cryst. Growth Des.*, 2011, **11**, 2942.
10 X. T. Wang, C. H. Liow, D. P. Qi, B. W. Zhu, W. R. Leow, H. Wang, X. D. Chen and S. Z. Li, *Adv. Mater.*, 2014, **21**, 3506.
11 L. Amy, G. Q. Lu, T. John and J. Yates, *Chem. Rev.*, 1995, **95**, 735.
12 B. Thompson and J. Fréchet, *Angew. Chem., Int. Ed.*, 2008, **47**, 58.
13 W. U. Huynh, J. J. Dittmer and A. P. Alivisatos, *Science*, 2002, **295**, 2425.
14 Z. Qiao, Z. L. Li and J. Y. Li, *J. Cryst. Growth*, 2009, **311**, 3651.
15 Q. Zhang, Q. A. Zhu and X. F. Sun, *Chin. J. Inorg. Chem.*, 2008, **24**, 547.
16 Y. Y. Zhu, P. Nie, L. F. Shen, S. Y. Dong, Q. Sheng, H. S. Li, H. F. Luo and X. G. Zhang, *Nanoscale*, 2015, **7**, 3309.
17 H. S. Hou, M. J. Jing, Z. D. Huang, Y. C. Yang, Y. Zhang, J. Chen and X. B. Ji, *ACS Appl. Mater. Interfaces*, 2015, **7**, 19362.
18 Y. B. Zhao and A. Manthiram, *Chem. Mater.*, 2015, **27**, 6139.
19 B. Li, H. Wang, B. W. Zhang, P. F. Hu, C. Chen and L. Guo, *ACS Appl. Mater. Interfaces*, 2013, **5**, 12283.
20 H. J. Zhang, M. Ge, L. T. Yang, Z. Zhou and W. Chen, *J. Phys. Chem. C*, 2013, **117**, 10285.
21 C. S. Yan, G. Chen, D. H. Chen and J. Pei, *CrystEngComm*, 2014, **16**, 3965.
22 Y. Li, X. Wei, B. Zhu, H. Wang, Y. Tang, T. C. Sum and X. Chen, *Nanoscale*, 2016, **8**, 11284.
23 Y. Li, J. Feng, H. Li, X. Wei, R. Wang and A. Zhou, *Int. J. Hydrogen Energy*, 2016, **41**, 4096.
24 Y. Li, X. Wei, X. Yan, J. Cai, A. Zhou, M. Yang and K. Liu, *Phys. Chem. Chem. Phys.*, 2016, **18**, 10255.
25 N. Maiti, S. H. Im, Y. H. Lee and S. I. Seok, *ACS Appl. Mater. Interfaces*, 2012, **4**, 4787.
26 S. S. Yao, J. Cui, Z. H. Lu, Z. L. Xu, L. Qin, J. Q. Huang, Z. Sadighi, F. Ciucci and J. K. Kim, *Adv. Energy Mater.*, 2017, **7**, 241.
27 G. Y. Chen, B. Deng and G. B. Cai, *J. Phys. Chem. C*, 2007, **112**, 672.
28 X. H. Xiong, G. H. Wang, Y. W. Lin, Y. Wang, X. Ou, F. H. Zheng, C. H. Yang, J. H. Wang and M. L. Liu, *ACS Nano*, 2016, **10**, 10953.
29 I. Moraseró and J. Bisquert, *J. Phys. Chem. Lett.*, 2010, **116**, 1579.
30 G. Y. Chen, B. Deng and G. B. Cai, *J. Phys. Chem. C*, 2008, **112**, 672.
31 S. S. Yao, J. Cui, Z. H. Lu, Z. L. Xu, L. Qin, J. Q. Huang, Z. Y. Sa, F. Ciucci and J. K. Kim, *Adv. Energy Mater.*, 2017, **7**, 1602149.
32 J. Yang, J. H. Zeng, S. H. Yu, L. Yang, Y. H. Zhang and Y. T. Qian, *Chem. Mater.*, 2000, **12**, 2924.
33 X. F. Duan, Y. Huang, Y. Cui, J. F. Wang and C. M. Liber, *Nature*, 2001, **409**, 66.
34 H. M. Huang, S. Mao, H. Feick, H. Yan, Y. Wu, H. Kind, E. Weber, R. Russo and P. D. Yang, *Science*, 2001, **292**, 1897.
35 C. An, K. Tang and Q. Yang, *Inorg. Chem.*, 2003, **42**, 8081.
36 B. Gates, B. Mayers, Y. Wu, Y. Sun and B. Cattle, *Adv. Funct. Mater.*, 2010, **10**, 679.
37 J. Tang and A. P. Alivisatos, *Nano Lett.*, 2006, **6**, 2701.
38 L. Tian, H. Y. Tan and J. J. Vittal, *Cryst. Growth Des.*, 2008, **8**, 734.
39 J. Ota, P. Roy, S. K. Srivastava, B. B. Nayak and A. K. Saxena, *Cryst. Growth Des.*, 2008, **8**, 6.
40 X. W. Zheng, Y. Xie, L. Y. Zhu, X. C. Jiang, Y. B. Jia, W. H. Song and Y. P. Sun, *Inorg. Chem.*, 2002, **41**, 455.
41 P. H. Zhang, C. X. Liu, X. L. Qi and X. Dai, *Nat. Phys.*, 2009, **5**, 438.
42 H. F. Dong, J. P. Lei, H. X. Ju, F. Zhi, H. Wang, W. Guo, Z. Zhu and F. Yan, *Angew. Chem., Int. Ed.*, 2012, **124**, 4685.
43 C. An, K. Tang and Q. Yang, *Inorg. Chem.*, 2003, **42**, 8081.
44 J. Kimling, M. Maier, B. Okenve, V. Kotaidis and H. Ballot, *Environ. Sci. Technol.*, 2006, **32**, 15700.
45 M. Zhou, L. Lei and Q. Dai, *Chem. Commun.*, 2007, 2645.
46 X. Tang, J. Qian, Z. Wang, H. Wang, Q. Feng and G. Liu, *J. Colloid Interface Sci.*, 2008, **330**, 386.
47 X. Yu, Z. Zhao, J. Zhang, W. Guo, L. Li, H. Liu and Z. L. Wang, *CrystEngComm*, 2017, **19**, 129.
48 H. Wang, Y. Bai, Q. Wu, W. Zhou, H. Zhang, J. Li and L. Guo, *Phys. Chem. Chem. Phys.*, 2011, **13**, 7008.
49 J. H. Pan, X. Z. Wang, Q. Huang, C. Shen, Z. Y. Koh, Q. Wang, A. Engel and D. W. Bahnemann, *Adv. Funct. Mater.*, 2014, **24**, 95.
50 J. Liu, Z. Guo, W. Wang, Q. Huang, K. Zhu and X. Chen, *Nanoscale*, 2011, **3**, 1470.
51 A. Hui, J. Ma, J. Liu, Y. Bao and J. Zhang, *J. Alloys Compd.*, 2017, **696**, 639.